Numerical Investigation of Delamination in Drilling of Carbon Fiber Reinforced Polymer Composites

Wenliang Tang[1] · Yan Chen[1] · Haojun Yang[1] ·
Hua Wang[1] · Qiwei Yao[1]

Abstract Drilling of carbon fiber reinforced polymer (CFRP) is a challenging task in modern manufacturing sector and machining induced delamination is one of the major problems affecting assembly precision. In this work, a new three-dimensional (3D) finite element model is developed to study the chip formation and entrance delamination in drilling of CFRP composites on the microscopic level. Fiber phase, matrix phase and equivalent homogeneous phase in the multi-phase model have different constitutive behaviors, respectively. A comparative drilling test, in which the cement carbide drill and unidirectional CFRP laminate are employed, is conducted to validate the proposedmodel in terms of the delamination and the similar changing trend is obtained. Microscopic mechanism of entrance delamination together with the chip formation process at four special fiber cutting angles (0°, 45°, 90° and 135°) is investigated. Moreover, the peeling force is also predicted. The results show that the delamination occurrence and the chip formation are both strongly dependent on the fiber cutting angle. The length of entrance delamination rises with increasing fiber cutting angles. Negligible delamination at 0° is attributed to the compression by the minor flank face. For 45° and 90°, the delamination resulted from the mode III fracture. At 135°, serious delamination which is driven by the mode I and III fractures is more inclined to occur and the peeling force reaches its maximum. Such numerical models can help understand the mechanism of hole entrance delamination further and provide guidance for the damage-free drilling of CFRP.

Keywords CFRP · Hole entrance delamination · Failure mechanisms · Finite element analysis

✉ Yan Chen
ninaych@nuaa.edu.cn

[1] College of Mechanical and Electrical Engineering, Nanjing University of Aeronautics and Astronautics, Nanjing 210016, China

1 Introduction

Carbon fiber reinforced polymer (CFRP), a kind of advanced composites, has been broadly used in various vital fields including aerospace, automobile and sports due to desirable mechanical properties such as high specific strength, high specific stiffness and corrosion resistance [1–3]. The increasing use of CFRP has placed higher demands on the machining operations. Unlike the conventional homogeneous metal materials, CFRP is a complex multi-phase, anisotropic material, which complicates the nature of the material removal in machining process [4]. Since drilling is the most frequently employed machining operation to produce riveted and bolted joints, the poor quality of machined holes impairs the precision of composite components severely [5]. With regard to drilling quality of CFRP, some drawbacks including the hole exit delamination (push-out delamination), hole entrance delamination (peel-up delamination), fiber pullout and hole burrs, always occur inevitably. Among these defects, the drilling-induced delamination at the exit and entry of the hole periphery are recognized as the most critical problems that lead to 60% of the component rejections [6].

In practice, it has been found that the push-out delamination was more severe than peel-up delamination [7]. Hence, many previous studies focused primarily on the hole exit delamination. Hole exit delamination which is mainly attributed to thrust force, has been widely and comprehensively covered in terms of experimental and theoretical analysis. It has been believed that there exists a critical thrust force below which no damage occurred [8–10]. On the contrast, hole entrance delamination occurs by sliding the first ply up the flutes of the drill [11]. Compared with the inner fibers that have enough supporting constraints, serious entrance delamination often takes place in the first ply inevitably. Konig et al. [12] explained that there was a peeling effect resulting from the periphery of the minor cutting edges. However, the peeling force leading to the entrance defect was rather difficult and even impossible to obtained.

Assuming that the material was isotropic, Hocheng et al. [13] proposed an analytical model of peel-up delamination by applying classical plate bending theory and linear elastic fracture mechanics to give conservative predictions for the critical peeling force. However, the peel-up model was hard to verify on the basis of the experimental data since the peeling force was barely measurable. Isbilir et al. [14] investigated the drilling process in CFRP with different cutting parameters and drawn a conclusion that the extent of delamination at hole entry rose with increase in feed rate and decreased with the increasing cutting speed. Nan et al. [15] carried out study on entrance spalling and found that the defect arose easily when the cutting direction and the fibers formed an angle of 45° during drilling CFRP and titanium alloy stacks. Choosing the full factorial plan, Karnik et al. [16, 17] analyzed the entrance delamination behavior by developing an artificial neural network model in which the affecting parameters like spindle speed, feed rate, and point angle were considered. Then the authors concluded that a combination of high speed, low values of feed rate and point angle was proved to be an appropriate selection for minimizing the entrance delamination. Obviously, experimental study which is exhaustive and time-consuming merely concentrated on quantitative characterization of the extent of hole entrance damage but lacked theoretical interpretation and mechanism analysis. In that case, the mechanism of entrance delamination cannot be fully understood so that this defect is still out of control during the machining.

Alternatively, the numerical approach has been utilized to simulate the cutting process in recent years. This promising approach played a pivotal role in analyzing cutting forces, fracture mechanisms and sub-surface damage in machining CFRP composites. Many recent research dealing with the simulation cutting process in composites, concentrated on two dimensional

orthogonal cutting model [18–21]. Compared with the two-dimensional (2D) model, the 3D model has advantages of simulating the cutting damage zone and delamination more exactly. Many attempts have been made in modeling the complex drilling process on the macroscopic level. On the basis of the Hashin's theory, Isbilir et al. [22, 23] and Phadnis et al. [24] both succeeded in predicting the entrance delamination by establishing the 3D finite element model of drilling CFRP. Macroscopic failure modes of the fiber and matrix were also presented during the drilling process. Feito et al. [25] developed the simplified model to study the delamination factor influenced by the stacking sequence, thrust force, and clamping. In these macroscopic simulation works, the entrance delamination zone could be predicted but the microscopic failures of workpiece could not be analyzed in detail. Accordingly, the microscopic numerical approach was adopted to study the microscopic failures of CFRP in different machining operations including drilling, milling and vibration-assisted cutting process [26–29]. The application of 3D microscopic simulation provides a new method for the study of the entrance delamination.

Currently, although many works regarding the micromechanical cutting model have been carried out, there are still few attempts focusing on the microscopic mechanism of the hole entrance delamination in drilling of CFRP. The objective of this research work is to investigate the mechanism of entrance delamination and the failures of each phase at various fiber cutting angles. The structure of this paper is organized as follows. Section 2 explains the microscopic approach to study the drilling-induced delamination and elaborates the procedures of building the 3D microscopic simulation model of CFRP drilling. Section 3 presents a description of the comparative trial to verify the numerical model. The chip formation process, mechanism of entrance delamination and numerical cutting forces are covered in Section 4. Finally, some conclusions are stated in the last section.

2 Finite Element Model

2.1 Model Establishment

According to the contact between cutting edges and workpiece, the entire drilling process can be divided into three stages as illustrated in Fig. 1. In Stage I, the chisel edge and main cutting edge gradually engage in the workpiece. In Stage II, cutting edges remove material in a steady state. In Stage III, the contact area between cutting edges and workpiece reduce gradually until drill bit penetrates out of the material completely. The gray shaded region is the interface region between Stage I and Stage II, at which the outer corner of drill bit begins to enter the workpiece and brings about the hole entrance delamination easily. The cutting process of the drill bit is essentially a combination of the orthogonal cutting of the minor cutting edge and the oblique cutting of the main cutting edge. The orthogonal cutting and oblique cutting models, as the simplification of the complex drilling process, offer a relatively simple method for the drilling research and have been widely used in the prediction of drilling forces and the analysis of machining defects [30–33].

In the numerical analysis of micro-failures, a complete drilling model will greatly increase the computational time and hardware costs. The outer corner of drill bit is the position where the main cutting edge meets the minor cutting edge. The integrity of the machined hole wall is directly affected by the minor cutting edges which have rarely been considered in the analysis of planar cutting mechanism. Moreover, the elementary cutting edge at the margin has a vital influence on the quality of hole entrance. In Fig. 2, the enlarged view of the cutting tool during drilling is shown. In order to carry out the simulation of the hole entrance delamination but

Fig. 1 Division of drilling stages
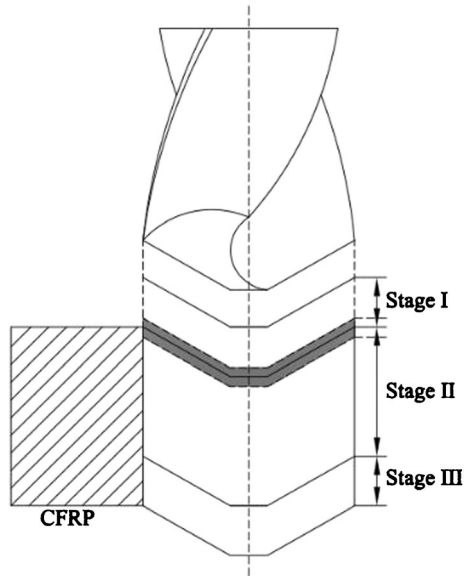
without losing the generality, the elementary cutting tool rather than the whole drill was selected as the research objective. Otherwise, the establishment of the simplified simulation model was based on the following assumptions:

1. The fibers obey the uniform distribution absolutely in the matrix.
2. Neglecting the effects induced by machining vibration.
3. Excluding the extension of delamination in Stages II and III.
4. The delamination formation is merely related with cutting edges at the outer corner in Stage I.

Owing to the specific ply direction in composites, cutting speed direction is varying relative to the fiber orientation at every moment. To distinguish various cutting modes, many scholars introduced the fiber cutting angle θ which was the relative angle between the direction of cutting speed and the ply orientation of uncut fibers, as shown in Fig. 3. At different angle positions, the specific energy was quite different and machining quality also changed greatly [34]. In the drilling process, as the drill rotates, the angle varies from 0° to 180° continuously. Within a range of fiber cutting angles from 0° to 180°, the models for four representative fiber cutting angles, that is, 0°, 45°, 90° and 135° were constructed separately in this study.
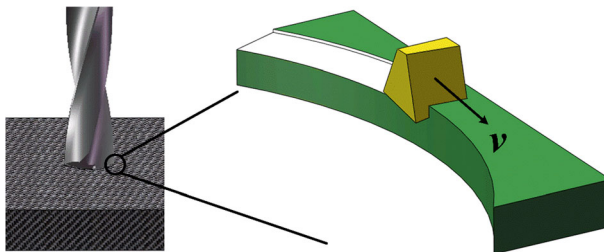
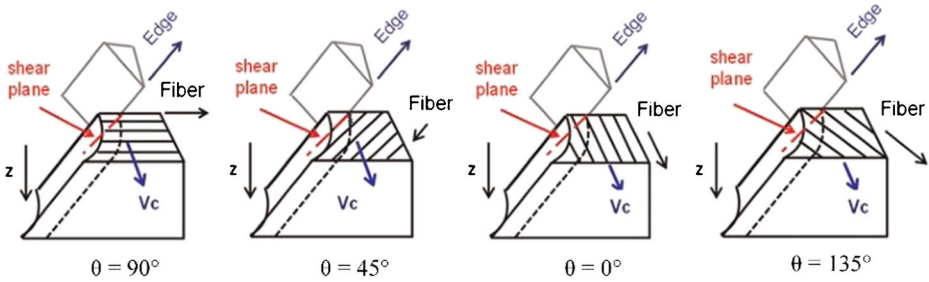**Fig. 2** Enlarged view of cutting at the outer corner of drill bit

Fig. 3 Definition of the fiber cutting angle θ in CFRP drilling [35]

2.2 Material Constitutive Behavior

Due to the nonhomogeneous and anisotropic nature of CFRP, the cutting zone is modeled as two individual phases, fiber and matrix. Considering the analysis efficiency and calculation rationality, the remaining bulk material far away from the cutting zone is treated as equivalent homogeneous material (EHM). Table 1 outlines the disparate material properties obtained from the open literature related to machining simulation of composites. Each phase has unique constitutive behavior which is of great importance for the accuracy of simulation.

The carbon fiber is modeled as a brittle and transverse isotropic material with five individual elastic constants. Fibers experience a linear elastic behavior before the onset of failure. Maximum principle stress criterion to indicate the fiber failure is implemented by means of the vectorized user material subroutine (VUMAT) to remove the distorted elements [20, 21, 36]. A flow chart detailing the flow of logic in the implementation of VUMAT is shown in Fig. 4. The subroutine is called for blocks of material points at each increment. When the subroutine is called, it is provided with state variables at the start of the increment. Once the criterion is satisfied, the element fails immediately and loses the load-carrying capacity absolutely. The EHM is defined as an anisotropic and pure elastic material whose mechanical properties are the same as macroscopic properties of CFRP.

The epoxy matrix is assumed to be an isotropic elastoplastic material [37, 38] and its constitutive behavior is given in Fig. 5. Elastic behavior is characterized by Young's Modulus and Poisson Ratio. Plastic behavior is described by von Mises yield criterion and isotopic hardening. Unlike the instantaneous failure of the brittle material, the stiffness of the elastoplastic material is gradually degraded as the load increases. Hence, progressive damage and failure are arranged for predicting the onset of failure and following damage during the

Table 1 Mechanical properties of CFRP composite [19, 21, 28]

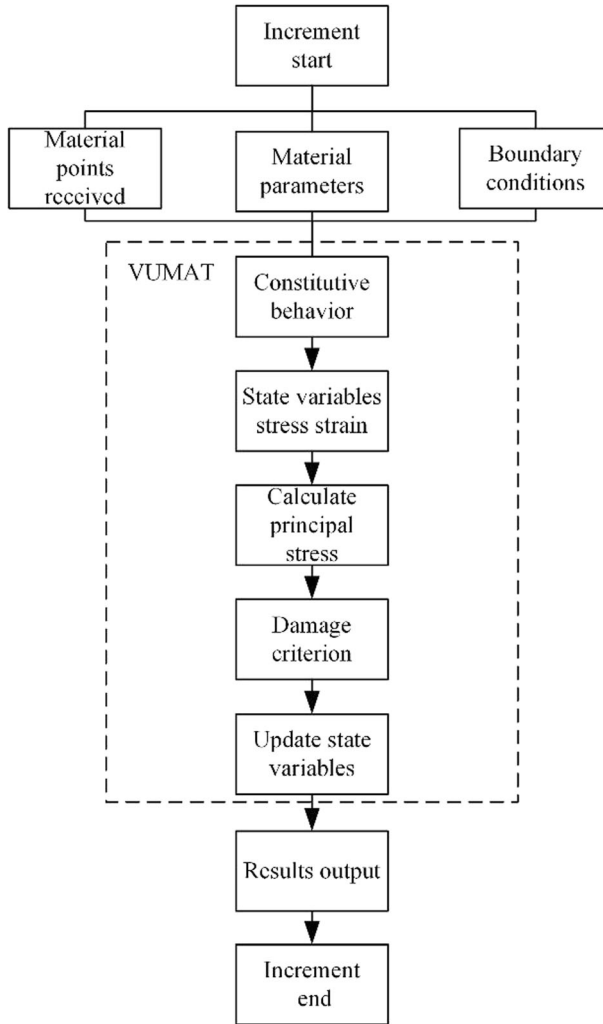| Materials	Properties	Values
Carbon fiber	Elastic constants	$E_{11} = 235$ GPa, $E_{22} = 14$ GPa, $\upsilon_{12} = 0.2$, $\upsilon_{23} = 0.25$ $G_{12} = 28$ GPa
	Tensile strength	$X_T = X_C = 3.59$ GPa
Matrix	Elastic constants	$E = 4$ GPa, $\upsilon = 0.4$
	Ultimate strength	$\sigma_b = 70$ MPa
	Yield strength	$\sigma_s = 27$ MPa
EHM	Elastic constants	$E_{11} = 142.184$ GPa, $E_{22} = E_{33} = 7.606$ GPa, $\upsilon_{12} = \upsilon_{13} = 0.28$, $\upsilon_{23} = 0.347$ $G_{12} = G_{13} = 4.151$ GPa, $G_{23} = 2.824$ GPa

Fig. 4 Simulation algorithm for implementation of VUMAT

matrix deformation. The material points appear to yield and harden after reaching the yield strength. According to Eq. (1), when the plastic strain accumulates to the initial failure strain ($\omega_D = 1$), the criterion for damage initiation is met.

$$\omega_D = \int \frac{d\bar{\varepsilon}^{pl}}{\bar{\varepsilon}_0^{pl}\left(-\dfrac{p}{q}, \dot{\bar{\varepsilon}}^{pl}\right)} \tag{1}$$

Where p is the hydrostatic stress, q is the Mises equivalent stress, $\bar{\varepsilon}^{pl}$, $\dot{\bar{\varepsilon}}^{pl}$, $\bar{\varepsilon}_0^{pl}$ are the equivalent plastic strain, the equivalent plastic strain rate and the equivalent plastic strain at the onset of damage, respectively.

After the damage occurs, the damage variable d which can be obtained through Eq. (2) and (3), evolves as the linear form damage evolution law. The equivalent displacement at failure
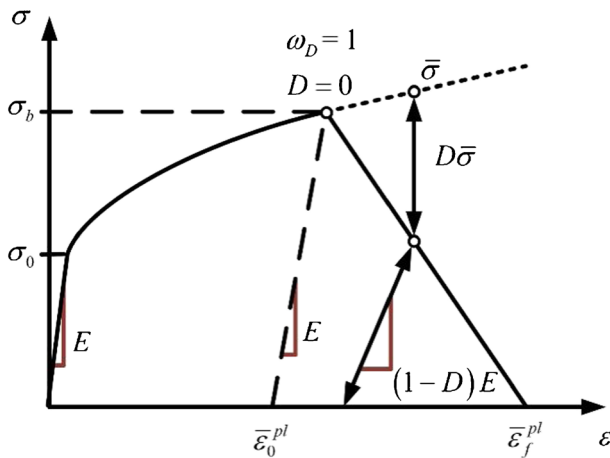
Fig. 5 Resin matrix constitutive behavior with progressive damage degradation

$\bar{u}_f^{pl}$ is computed on the basis of the fracture energy dissipation per area G_f which is specified in the model.

$$d = \frac{L\dot{\bar{\varepsilon}}^{pl}}{\bar{u}_f^{pl}} = \frac{\dot{\bar{u}}^{pl}}{\bar{u}_f^{pl}} \tag{2}$$

$$\bar{u}_f^{pl} = \frac{2G_f}{\sigma_b} \tag{3}$$

Where the characteristic length of the element L can alleviate the mesh dependency of the simulation results and σ_b is the yield stress at failure.

At any given time increment during the analysis, the degraded elastic modulus E can be deduced from the scalar damage equation Eq. (4):

$$E = (1-D)E_0 \tag{4}$$

$$\sigma = (1-D)\bar{\sigma} \tag{5}$$

where E_0 is the initial elastic modulus and the overall damage variable D is equal to d when the single damage mode is used. When D reaches 1, the element is removed from the mesh and offers no subsequent resistance to deformation.

2.3 Simulation Procedure

ABAQUS is a very powerful finite element software for handling nonlinear dynamics problems and widely used in numerical cutting simulation. A 3D cutting model of hole entrance damage at fiber cutting angle 90° was developed by ABAQUS, as presented in Fig. 6. As the stiffness of the cemented carbide tool was much greater than that of the workpiece, the tool could be safely regarded as a rigid body. The cutting speed of the reference
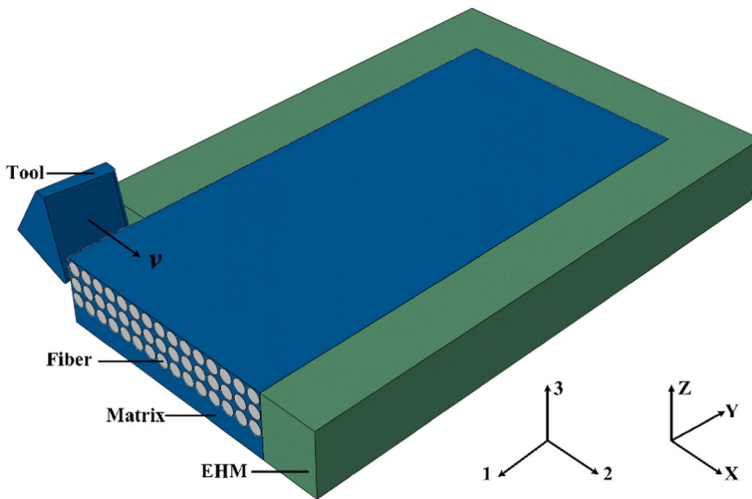
Fig. 6 Schematic representation of the finite element model ($\theta = 90°$)

point was 0.5 m/s, the same value used in the trial test. The geometry parameters of the cutting edge at the outer corner were obtained by the Walter Helicheck Pro measuring instrument. The nose radius of double edges was 2 μm. According to the feed rate and the major cutting edge angle, the length of the major cutting edge was set equal to 69.3 μm while other remaining parameter values are outlined in Table 2. Otherwise, the microscopic simulation time was definitely short, so the negligible change of chip thickness and heat transfer between the tool and workpiece were both neglected. The average uncut chip thickness was 15 μm, identical to the feed per tooth in the verification test.

The fiber phase had a uniform distribution in the matrix phase. Fiber volume of the CFRP composite used in the simulation was 60% and fiber diameter was 7 μm. To ensure the identical cutting width perpendicular to the speed direction at four fiber cutting angles, the workpiece shape was set as rectangle at 0° and 90° and parallelogram at 45° and 135°, separately. The orientation of fiber phase was defined through the local material coordinate system in which 1 axis was the principle direction of fibers, 2 axis was perpendicular to 1 axis and lied in the laminate plane, 2–3 plane was the isotropy plane. Meanwhile, a velocity coordinate system was also created. X axis was the in the speed direction, Z axis was in the same direction of the 3 axis. Two coordinates were both under the right-hand law, as shown in the lower-right corner of the Fig. 6.

The mesh in the micromechanical area was realized by utilizing hexagonal elements with eight nodes and reduce integration (C3D8R). The global seed size was 1.5 μm. The ten nodes modified quadratic tetrahedron elements (C3D10M) was applied for meshing the tool whose shape was irregular. Coarse mesh with C3D8R elements was allocated to the EHM so as to

Table 2 Tool geometry parameters

Normal rake angle	Normal flank angle	Minor flank angle	Inclination angle	Major cutting edge angle	Minor cutting edge angle
15.1°	10.7°	0.9°	5.0°	77.5°	0°

prevent the elevated computational cost of the analysis. In addition, the encastre and symmetry boundary conditions were applied at the bottom and surrounding face correspondingly to restrict the displacements. The coefficient of friction between the tool and workpiece was dependent on the fiber cutting angle [39]. The value was taken as 0.3, 0.6, 0.8, 0.6 at 0°, 45°, 90°, 135° fiber cutting angles, respectively.

Although the EHM approach has been used to minimize the computational time, the number of elements in this simulation was still so large, about 700,000, that the whole analysis process was always significantly complex and time-consuming. In order to speed up the operation further, the mass scaling factor was applied in the simulation analysis on the premise of little influence over the accuracy of results. The factor can increase the global stability limit and reduce the increments required to perform the analysis.

3 Experimental Work

3.1 Experimental Setup

The details of numerical model were described in the previous section. This section presents the comparative test to validate the above model in terms of the delamination damage. Drilling trial was conducted on the DMU mono block machining center under dry cutting conditions, as illustrated in Fig. 7a. The adopted revolution velocity was 2000 rpm and feed rate was equal to 60 mm/min. A cemented carbide drill with 4.763 mm diameter and 15.0° helix angle was employed to machine four holes in the operation, as shown in Fig. 7b.

The main focus in this work is only delamination at the hole entrance, so workpiece material was unidirectional CFRP laminate with a small thickness of 2.5 mm. Powder chips were collected by vacuuming cleaner equipment timely to avoid the pollution and negative impacts on individuals' health. Besides, the delamination forming process was monitored through the Photron high speed camera with maximum frequency of 30,000 fps. To clearly observe the local damage, the delamination measurement was done by using the Hirox KH-

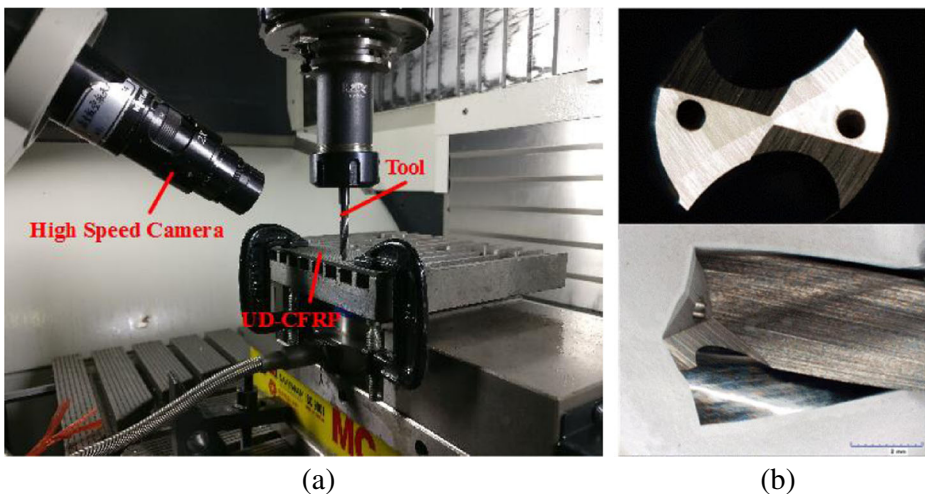(a)   (b)

Fig. 7 The experimental details of drilling CFRP **a** Experimental setup of CFRP drilling **b** Views of the drill

7700 3D optical microscope with a resolution of 0.01 μm. In a half-revolution of the drill bit, the fiber cutting angle θ at the top view continuously changed from 180° to 0°, as depicted in Fig. 8. Because of the periodic change of fiber cutting angle, the damage always occurred symmetrically on the hole periphery [35]. At the particular angle, the average length L_θ of the entrance delamination was defined via the following equation:

$$L_\theta = (R_1 + R_2 - D_0)/2 \tag{6}$$

where R_1, R_2 are the radius of delamination at symmetrical positions and D_0 is the nominal hole diameter as shown in Fig. 9. In this test, the average delamination length at the specific angle was calculated at all holes.

3.2 Validation of Entrance Delamination

As for the simulation results, in order to alleviate the influence of the boundary conditions on the damage size absolutely, the quantitative characterization of damage excluded the first two fibers adjacent to the workpiece boundary. During the load transfer, the propagation of matrix failure was always more severe than the fiber failure due to the lower strength Consequently, the average length of entrance delamination was represented by the matrix damage zone. The field output variable DUCTCRT denoted the criterion for damage initiation. As depicted in Fig. 10, the average delamination length orthogonal to the speed direction was measured from the trim plane of the minor cutting edge in the ABAQUS. In those simulation models, it was evident that the material removal process at 135° was not beneficial to the favorable hole quality.

At the interface region between Stage I and Stage II, Fig. 11 shows the formation process of entrance delamination recorded by high speed camera. The entrance delamination occurred at around 135°. During the Stage I, the major cutting edge of the drill abraded the composite laminate firstly. As the drill bit cut into the composite laminate, the major cutting edge length participating in the cutting behavior increased gradually. The geometric transition between the elementary cutting tools extracted from the major was pretty smooth, so the material removal process was somewhat steady, hardly forming serious machining defects in the machined

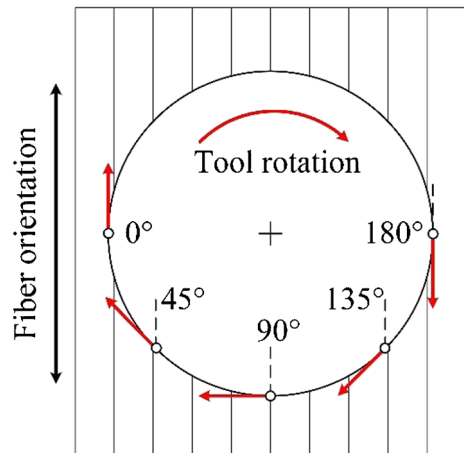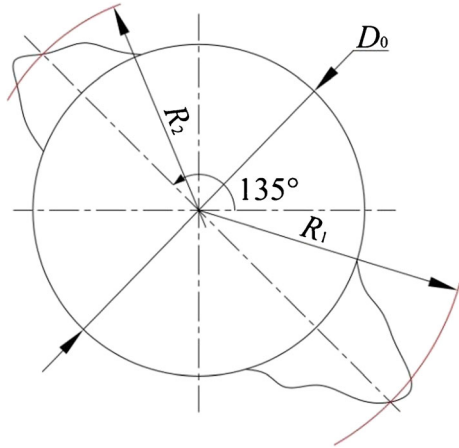**Fig. 8** Top view of the hole entrance

Fig. 9 The measurement of delamination length $L_\theta(\theta = 135°)$

smooth surface. At the end of Stage I, the minor cutting edge at the outer corner where sharp geometric change happened, began to contact with the laminate. The cutting mode converted from the major edge cutting individually to a couple of edges cutting simultaneously. In Fig. 11b, the fiber material that was not chopped by the minor cutting edge sufficiently tended to spiral up along the flutes at the position of 135°. The peeling force, generating in the axial direction through the slope of the drill bit flutes, separated the piles from the uncut portions and induced a delamination zone around the hole entry periphery.

As it can be observed from Fig. 12, there exist uncut fibers at 135° and peeled up fibers at 90° while few damages occur at the angle ranging from 0° to 90°. The delamination position mainly concentrated at about 135° where the extent of damage was much larger than that of other positions. Similar damage observations were also found in [35, 40]. At each angle, the delamination length was 20.16 μm, 30.31 μm, 80.56 μm, 179.63 μm, respectively.

Figure 13 shows a comparison between the experimental and numerical entrance delamination. Obviously, the simulation presents a same upward trend as the experiment does. In each case, the entrance damage increases slightly with fiber cutting angles up to 90°, after which it rises sharply to reach its maximum at 135°. At 0° and 45°, the numerical predictions are almost the same as the counterparts of test. At 90° and 135°, the numerical predictions are lower than experimental values. The deviations can be explained as follows. Firstly, the heat generation by plastic deformation is ignored in the numerical analysis while the high cutting temperature in the comparative test will lead to matrix softening. When the fibers lose supporting constraints, the delamination is definitely easier to expand. Moreover, limited by the scale of simulation models, tool displacement is much smaller. The entrance delamination will further propagate during the Stages II and III which is not taken into account in simulations. In Fig. 12d, there have been plenty of fibers accumulating on the rake face. The exposing fibers will continue to be peeled up in an extreme case where the cutting path is long enough and the delamination length will be larger than 82.45 μm. Considering the various sources of the difference, it can be safely concluded that the numerical model can estimate the extent of damage reasonably and be used to explain the formation of hole entrance delamination.
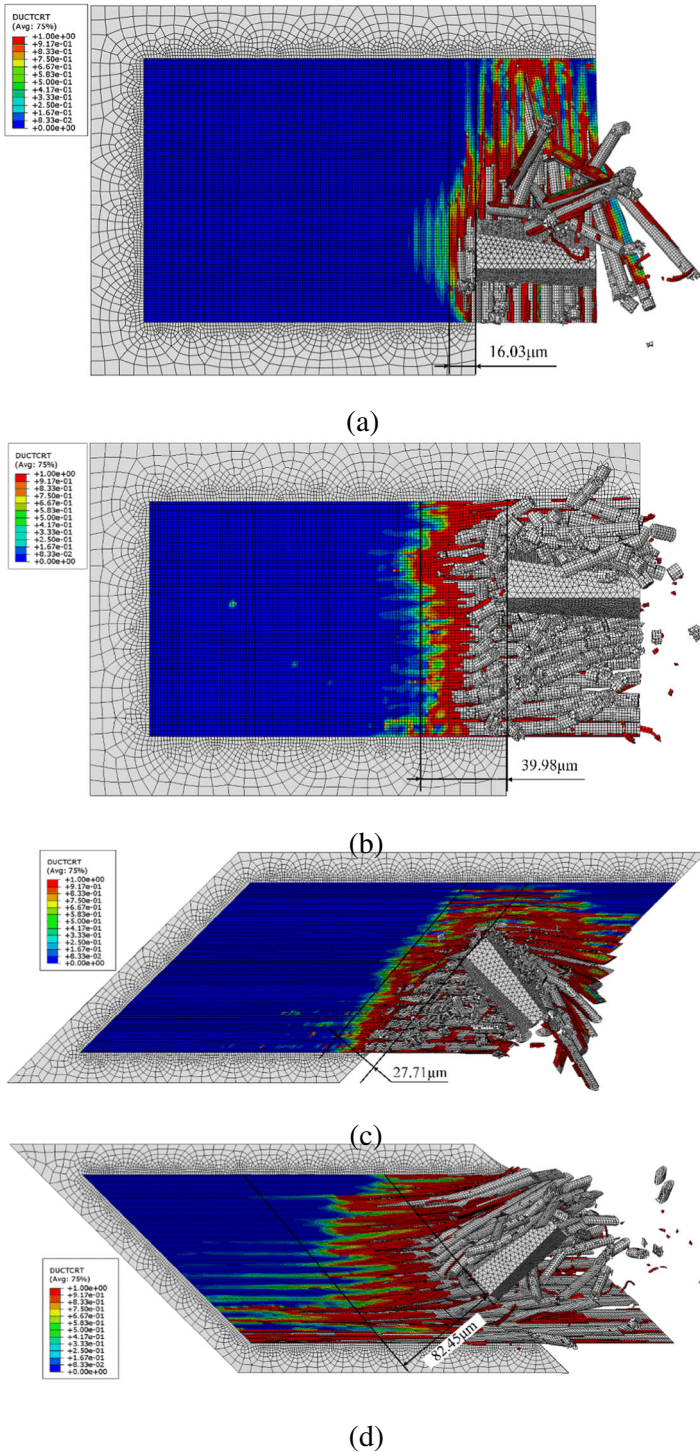
(a)

(b)

(c)

(d)

Fig. 10 Delamination measured in the numerical models **a** $\theta = 135°$ **b** $\theta = 90°$ **c** $\theta = 45°$ **d** $\theta = 0°$

4 Results and Discussion

4.1 Analysis of Chip Formation Process

The CFRP material removal process is accompanied by the micro-failures of fibers and matrix. When the tool contacts the workpiece, the local matrix compressed by the tool always fails firstly due to the lower strength. Fig. 14a shows the simulation result for the 0° orientation. With the tool moving forward, the fibers are peeled up and separated from matrix. The fibers, under the compressive load, begin to bend and slip along the rake face while the bending stress gradually increases until exceeding the fiber bending strength to break. Due to the thin uncut chip thickness, most brittle fibers turn into long chips in the cutting path and a few powder-like chips are formed resulting from the tool crushing.

In the circumstance of 45°, the fiber orientation and cutting speed direction is not parallel to each other. The tool tip penetrates into the workpiece with an angle and the workpiece is subjected to the concentrated force at the beginning. As shown in Fig. 14b, such stress concentration at the local tip-workpiece contact zone brings about a shear failure along the trim plane. As the tool advances, most fibers are sheared off neatly at the vicinity of the minor cutting edge. Meanwhile, the rake face continues to press the broken fibers that are easier to flow along the flutes toward the machined hole due to the presence of the positive inclination
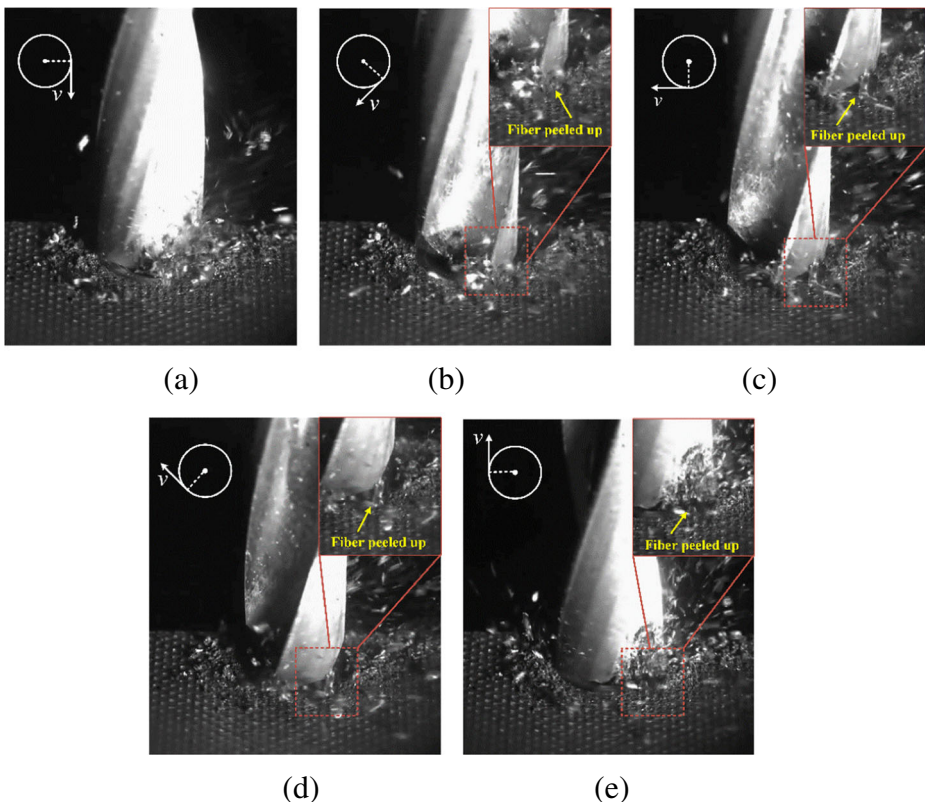

(a)   (b)   (c)

(d)   (e)

Fig. 11 The formation process of delamination in a half-revolution of drill bit **a** $\theta = 180°$ **b** $\theta = 135°$ **c** $\theta = 90°$ **d** $\theta = 45°$ **e** $\theta = 0°$
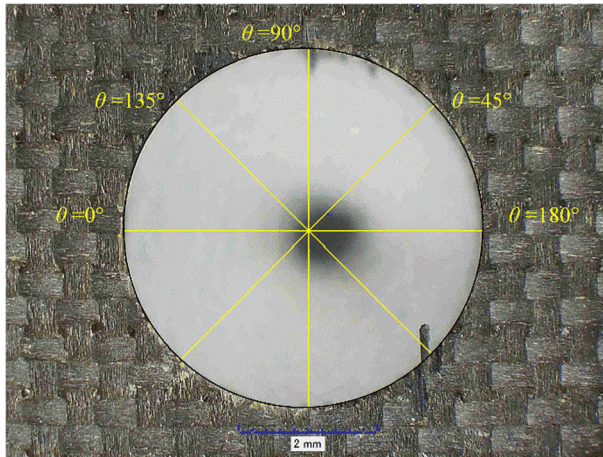
Fig. 12 Hole entrance delamination in the comparative test

edge. The normal and friction forces from the rake face are insufficient to cause subsequent damages of fibers. Eventually long chips with almost identical length are formed.

For the case of 90°, the fiber failure is dominated by the crushing at first and followed by the bending fracture, as exhibited in Fig. 14c. The fibers bear the concentrated force initially from the minor cutting lip. With the motion of the cutting tool, the inclination edge is quite small, hence the point force changes into the uniform force applied by the main cutting edge and the rake face. The fibers in the proximity of the rake face appear to break at the uncut material side where the bending stress is exactly equal to the ultimate bending strength finally. On one hand, the point force from the minor cutting lip and the crushing from the main cutting lip bring about the grainy chips. On the other hand, the uniform force appearing later cause the longer chips on the rake face.

Different from the three situations above, the fiber failure is mainly the bending fracture at 135°. In this condition, a larger angle is formed between the fiber and speed orientations. Instead of the minor cutting edge, the rake face contacts the workpiece firstly and exercises an
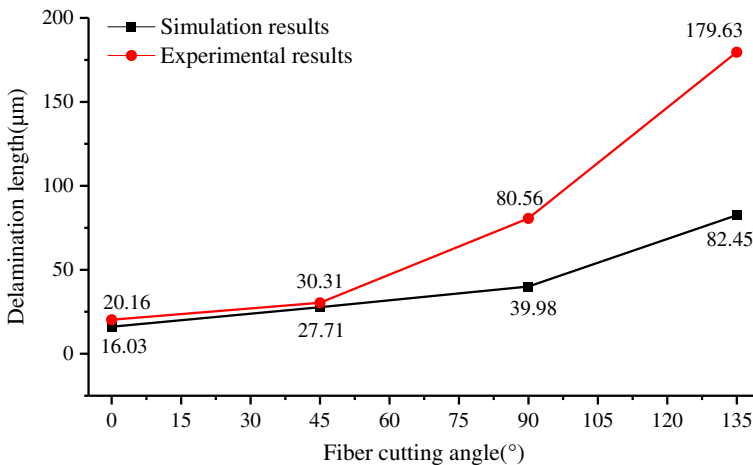

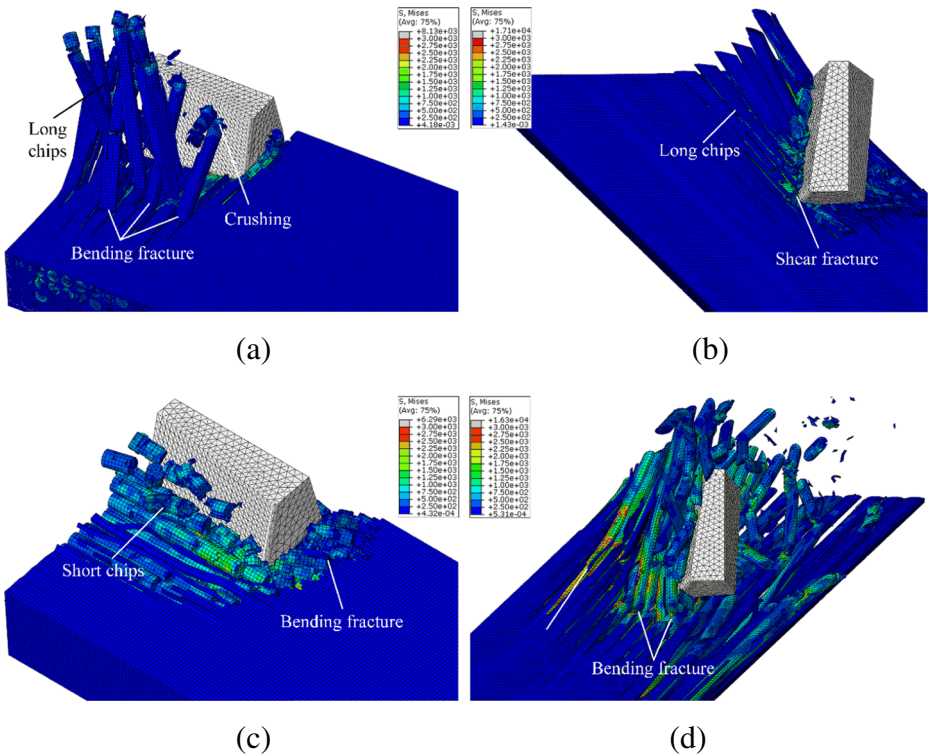**Fig. 13** Comparison of the simulation and experimental results

Fig. 14 Fiber failure modes during the chip formation process **a** $\theta = 0°$ **b** $\theta = 45°$ **c** $\theta = 90°$ **d** $\theta = 135°$

even force on the fibers in the cutting zone. Unlike the concentrated force chopping the fiber easily, the uniform force gives rise to considerable bending deflection. The chips will not be produced only if the fibers are not cut off completely. Some fibers are lifted up at the uncut area away from the hole entry periphery and others form few continuous chips after undergoing severe peeling and spalling, as shown in Fig. 14d. In the developed models, not only the chip morphologies and fiber failure modes with different angles were consistent with some experimental orthogonal cutting cases [41–43], but also the material removal mechanism responsible for the delamination occurrence was assessed more comprehensively in drilling of CFRP.

4.2 Mechanism of Entrance Delamination Formation

The occurrence of damage is simultaneous with the chip formation process. For the case of 0°, the fiber orientation is parallel with speed direction and the exerted cutting force is mainly in the fiber orientation. There exists almost no cutting force in the transverse direction. Although the transverse strength of the fiber is much lower than the longitudinal strength, the transverse cutting force is not enough to provoke ruptures of fibers near the minor flank face. The small-area matrix damage is primarily attributed to the normal load from the minor flank face and the compression among fibers, as shown in Fig. 15a. Consequently, the delamination extends negligibly along the transverse direction. The delamination length is equal to 16.03 μm in the end.

As for the 45°, in the uncut area, the fibers bear the force from the minor flank face. The mode III fracture results in some micro cracks, as shown in Fig. 15b. Because the fibers can be cut off promptly and completely, only a little local delamination expansion produced, 27.71 μm approximately.

Figure 15c illustrates the delamination observed in the 90° simulation. The mode I fracture appears in the resin-rich area and develops along the fiber orientation. In the meantime, the debonding between the two phases in the fiber direction arises from the mode III fracture. The sizeable deflection will not emerge because of the strong supporting constraints in the deflection direction. Some short fibers are pulled out at the hole entrance. In the end, the length of damage is approximately equal to 39.98 μm.

In terms of the delamination formation, the 135° is also rather different from the other three instances. As the tool approaches, the machined incompletely fibers accumulate on the rake face. In such a case, the out-of-plane displacement of the fibers will become larger and larger before the fracture takes place. The bending fracture occurs at the place where the radius of curvature at failure is reached. Some fibers that contact with the rake face earlier, experience several damages after massive displacement and others tend to be pulled up along the rake face continually. In this regard, the onset and propagation of delamination by bending load is dominated by the mode I and III fractures. Distinguished from the bending deformation in 90°, the deflection is in the direction oriented perpendicularly to the first ply and the deformed fibers are short of good supporting constraints.
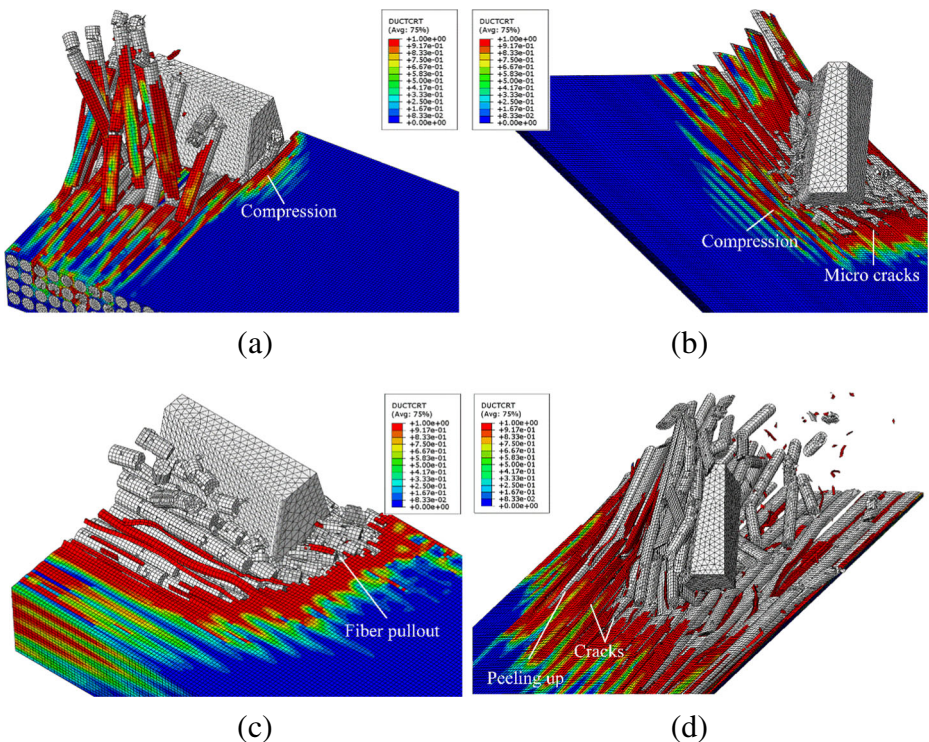

Fig. 15 Mechanism of entrance delamination formation **a** $\theta = 0°$ **b** $\theta = 45°$ **c** $\theta = 90°$ **d** $\theta = 135°$

Furthermore, under the coupling influences of the mode I and III fractures, the matrix surrounding the deformed fibers tend to fail in a direction congruent with the fiber orientation. Meanwhile, the fibers at 135° are easier to be peeled up and separate so dramatically that a great deal of cracks take place at the uncut zone, as shown in Fig. 15d. Finally, with the deterioration of defects, the entrance delamination reaches about 82.45 μm which is larger than that of other cases. The 135° position is more prone to the delamination, which is in accordance with the phenomenon recorded by the high speed camera.

4.3 Analysis of Cutting Forces

Cutting forces, which are important parameters in the cutting process, have direct influence on the cutting heat, tool life and machining quality. In the experimental machining, the peeling force which leads to the formation of entrance delamination cannot be measured. Conversely, the simulation cutting forces can be conveniently output, which provide a reference for the analysis of machining defects. Cutting forces of the whole elementary tool could be decomposed in three components: the cutting force F_x forming the torque, the radial force F_y and the feed resistance force F_z. Likewise, contact forces between the rake face and workpiece can be divided into three component forces: F_{rx}, F_{ry}, F_{rz}. The subscripts x, y, z represented the axis directions in the velocity coordinate system, as shown in Fig. 6. Additionally, it is noted that average cutting forces over the whole analysis have been converted to the forces per cutting width with an average uncut chip thickness of 15 μm.

Figure 16 shows the effects of fiber cutting angles on the cutting forces. The forces experience significant changes because of the nonhomogeneous and anisotropic nature of CFRP. Moreover, the fluctuation reflects the fiber failure and fracture propagation modes during the chip formation process. The feed resistance force F_z mainly reflects the contact between the flank face and the bottom trimmed face. Since the instantaneous uncut chip thickness keeps constant in the simulation model, F_z is not obviously affected by the angle and exhibits few overall changes which could be attributed to bounce back of the machined material. The interaction between the minor flank face and the machined hole wall forms the radius force F_y which changes in a small range. Different from the two forces described above, the main cutting force F_x is drastically affected by the fiber cutting angle and shows an upward trend. The cutting force F_x and the radial force F_y both reach the peak at 135°. In this regard, a number of unbroken fibers that accumulated in the cutting path gradually resulted in a larger load.

Contact forces from the rake face include the contact pressures and frictional forces. In Fig. 17, the relations of contact forces versus the fiber cutting angles are plotted. The peeling force F_{rz} shows higher values at 0° and 135° because of the pronounced bending deformation. The maximum peeling force proves the serious peel-up delamination at 135°. In contrast, smaller peeling forces appear at 45° and 90° accounting for the less delamination. Similarly, F_{ry} also reaches its summit because lots of broken fibers scratch the tool rake face continuously. Besides, the chips flow along the flutes frequently at 45°, which leads to the larger value of F_{ry}. As for the main contact force F_{rx}, it implies the mode III fracture dominating the formation of entrance delamination for all occasions except 0°. With the rise of the fiber cutting angle, F_{rx} increases almost linearly, which can be ascribed to the rising compressive load on the rake face.
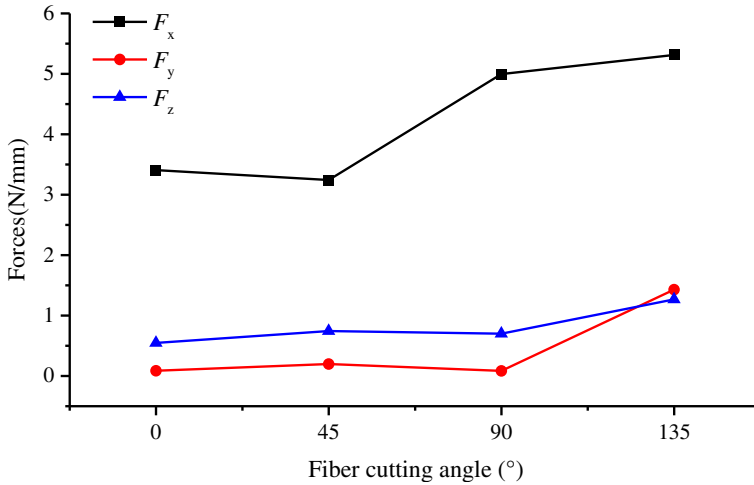
Fig. 16 Variation of tool cutting forces versus the fiber cutting angles

5 Conclusions

In this study, a new 3D microscopic model has been successfully established to explore microscopic failures of fiber and matrix phase in delamination and the chip formation process. And, some conclusions can be drawn as follows:

(1) Fiber cutting angles are observed to play a crucial role in determining the entrance delamination and chip formation. In terms of the chip formation, the fibers are both cut off easily by the tool tip due to the concentrated forces for the fiber cutting angle of 45° and 90°. At 0° and 135°, the fibers mainly bear uniform resistance force from the rake face. At 135°, the uniform force from the rake face is more probable to bring about large bending deformation so that the chip breakout barely occurs.
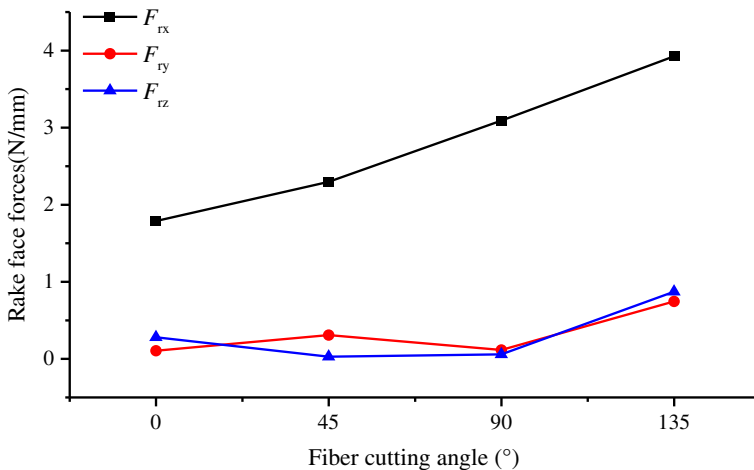

Fig. 17 Variation of contact forces versus the fiber cutting angles

(2) As for the entrance delamination, in 0°, 45°, and 90° cases, the fibers around the hole entry broke easily through various failure modes to form different types of chips. Therefore, there is little chance for the delamination occurrence. In contrast, the position of 135° is a vulnerable location at which the peel-up damage reaches its worst. In the 0° case, the negligible damage zone is attributed to compression. In other three cases, the mode III fracture always exist during the onset and propagation of delamination. In addition, the mode I fracture also dominates the damage at 135°.

(3) The predicted peeling force in the numerical models compensates for the weakness of drilling experiments successfully. The peeling force reaches its maximum at 135°, which can account for the serious entrance delamination. Furthermore, according to the predicted results, the analytical model of delamination can be developed further, which will be the focus of future research work.

References

1. Dandekar, C.R., Shin, Y.C.: Modeling of machining of composite materials: A review. J. Mach. Tools. Manuf. **57**(2), 102–121 (2012)
2. Soutis, C.: Fibre reinforced composites in aircraft construction. Prog. Aerosp. Sci. **41**(2), 143–151 (2005)
3. Dong, C.: Development of a Model for predicting the transverse coefficients of thermal expansion of unidirectional carbon fibre reinforced composites. Appl. Compos. Mater. **15**(3), 171–182 (2008)
4. Che, D., Saxena, I., Han, P., Guo, P., Ehmann, K.F.: Machining of carbon fiber reinforced plastics/polymers: A literature review. ASME. J. Manuf. Sci. Eng. **136**(3), 034001 (2014)
5. Santiuste, C., Barbero, E., Miguélez, M.H.: Computational analysis of temperature effect in composite bolted joints for aeronautical applications. J. Reinf. Plast. Compos. **30**(1), 3–11 (2011)
6. Stone, R., Krishnamurthy, K.: A neural network thrust force controller to minimise delamination during drilling of graphite-epoxy laminates. J. Mach. Tools. Manuf. **36**(9), 985–1003 (1996)
7. Shyha, I., Soo, S.L., Aspinwall, D., Bradley, S.: Effect of laminate configuration and feed rate on cutting performance when drilling holes in carbon fibre reinforced plastic composites. J. Mater. Process. Technol. **210**(8), 1023–1034 (2010)
8. Hocheng, H., Tsao, C.C.: The path towards delamination-free drilling of composite materials. J. Mater. Process. Technol. **167**(2–3), 251–264 (2005)
9. Karimi, N.Z., Heidary, H., Minak, G.: Critical thrust and feed prediction models in drilling of composite laminates. Compos. Struct. **148**, 19–26 (2016)
10. Ojo, S.O., Ismail, S.O., Paggi, M., Dhakal, H.N.: A new analytical critical thrust force model for delamination analysis of laminated composites during drilling operation. Compos. Part. B-Eng. **124**, 207–217 (2017)
11. Girot, F., Dau, F., Gutiérrez-Orrantia, M.E.: New analytical model for delamination of CFRP during drilling. J. Mater. Process. Technol. **240**, 332–343 (2017)
12. König, W., Graß, P.: Quality Definition and assessment in drilling of fibre reinforced thermosets. Ann. CIRP. **38**(1), 119–124 (1989)
13. Ho-Cheng, H., Dharan, C.K.H.: Delamination during drilling in composite laminates. Trans. ASME. J. Eng. Ind. **112**(3), 236–239 (1990)
14. Isbilir, O., Ghassemieh, E.: Delamination and wear in drilling of carbon-fiber reinforced plastic composites using multilayer TiAlN/TiN PVD-coated tungsten carbide tools. J. Reinf. Plast. Compos. **31**(10), 717–727 (2012)
15. Nan, C., Wu, D., Gao, Y., Ma, X., Chen, K.: Influence of metal chips on drilling quality of carbon fiber reinforced plastic and titanium stacks. In: IEEE International Conference on Cyber Technology in Automation, Control, and Intelligent Systems. pp. 1204–1209. Shenyang, China (2015)

16. Karnik, S.R., Gaitonde, V.N., Rubio, J.C., Correia, A.E., Abrão, A.M., Davim, J.P.: Delamination analysis in high speed drilling of carbon fiber reinforced plastics (CFRP) using artificial neural network model. Mater. Des. **29**(9), 1768–1776 (2008)

17. Gaitonde, V.N., Karnik, S.R., Rubio, J.C., Correia, A.E., Abrão, A.M., Davim, J.P.: Analysis of parametric influence on delamination in high-speed drilling of carbon fiber reinforced plastic composites. J. Mater. Process. Technol. **203**(1–3), 431–438 (2008)

18. Pecat, O., Rentsch, R.D., Garbrecht, M., Brinksmeier, E.: Modeling and simulation of the machining of unidirectional CFRP. Adv. Mater. Res. **907**, 55–62 (2014)

19. Rao, G.V.G., Mahajan, P., Bhatnagar, N.: Micro-mechanical modeling of machining of FRP composites – cutting force analysis. Compos. Sci. Technol. **67**(3–4), 579–593 (2007)

20. Rao, G.V.G., Mahajan, P., Bhatnagar, N.: Machining of UD-GFRP composites chip formation mechanism. Compos. Sci. Technol. **67**(11), 2271–2281 (2007)

21. Abena, A., Soo, S.L., Essa, K.: Modelling the orthogonal cutting of UD-CFRP composites: Development of a novel cohesive zone model. Compos. Struct. **168**, 65–83 (2017)

22. Isbilir, O., Ghassemieh, E.: Finite element analysis of drilling of carbon fibre reinforced composites. Appl. Compos. Mater. **19**(3–4), 637–656 (2012)

23. Isbilir, O., Ghassemieh, E.: Numerical investigation of the effects of drill geometry on drilling induced delamination of carbon fiber reinforced composites. Compos. Struct. **105**(8), 126–133 (2013)

24. Phadnis, V.A., Makhdum, F., Roy, A., Silberschmidt, V.V.: Drilling in carbon/epoxy composites: Experimental investigations and finite element implementation. Compos. Part. A-Appl. Sci. Manuf. **47**(1), 41–51 (2013)

25. Feito, N., López-Puente, J., Santiuste, C., Miguélez, M.H.: Numerical prediction of delamination in CFRP drilling. Compos. Struct. **108**(1), 677–683 (2014)

26. Gao, C., Xiao, J., Xu, J., Ke, Y.: Factor analysis of machining parameters of fiber-reinforced polymer composites based on finite element simulation with experimental investigation. Int. J. Adv. Manuf. Technol. **83**(5–8), 1113–1125 (2016)

27. Xu, W., Zhang, L., Wu, Y.: Effect of tool vibration on chip formation and cutting forces in the machining of fiber-reinforced polymer composites. Mach. Sci. Technol. **20**(2), 312–329 (2016)

28. Calzada, K.A., Kapoor, S.G., Devor, R.E., Samuel, J., Srivastava, A.K.: Modeling and interpretation of fiber orientation-based failure mechanisms in machining of carbon fiber-reinforced polymer composites. J. Manuf. Process. **14**(2), 141–149 (2012)

29. Wang, F., Wang, X., Yang, R., Gao, H., Su, Y., Bi, G.: Research on the carbon fibre-reinforced plastic (CFRP) cutting mechanism using macroscopic and microscopic numerical simulations. J. Reinf. Plast. Compos. **36**(8), 555–562 (2016)

30. Luo, B., Li, Y., Zhang, K., Cheng, H., Liu, S.: A novel prediction model for thrust force and torque in drilling interface region of CFRP/Ti stacks. Int. J. Adv. Manuf. Technol. **81**(9–12), 1497–1508 (2015)

31. Lazar, M.B., Xirouchakis, P.: Mechanical load distribution along the main cutting edges in drilling. J. Mater. Process. Technol. **213**(2), 245–260 (2013)

32. Naisson, P., Rech, J., Paris, H.: Analytical modeling of thrust force and torque in drilling. Proc. Inst. Mech. Eng. B J. Eng. Manuf. **227**(10), 1430–1441 (2013)

33. Zitoune, R., Collombet, F., Lachaud, F., Piquet, R., Pasquet, P.: Experiment–calculation comparison of the cutting conditions representative of the long fiber composite drilling phase. Compos. Sci. Technol. **65**(3–4), 455–466 (2005)

34. An, Q., Ming, W., Cai, X., Chen, M.: Study on the cutting mechanics characteristics of high-strength UD-CFRP laminates based on orthogonal cutting method. Compos. Struct. **131**, 374–383 (2015)

35. Bonnet, C., Poulachon, G., Rech, J., Girard, Y., Costes, J.P.: CFRP drilling: Fundamental study of local feed force and consequences on hole exit damage. J. Mach. Tools. Manuf. **94**, 57–64 (2015)

36. Han, G., Guan, Z., Li, Z., Du, S.: Microscopic progressive damage simulation and scale-span analysis of cross-ply laminate based on the elastic–plastic theory. Appl. Compos. Mater. **22**(1), 1–12 (2015)

37. Hobbiebrunken, T., Fiedler, B., Hojo, M., Ochiai, S., Schulte, K.: Microscopic yielding of CF/epoxy composites and the effect on the formation of thermal residual stresses. Compos. Sci. Technol. **65**(10), 1626–1635 (2005)

38. Ren, Y., Zhang, S., Jiang, H., Xiang, J.: Meso-scale progressive damage behavior characterization of triaxial braided composites under quasi-static tensile load. Appl. Compos. Mater. 1–18 (2017). https://doi.org/10.1007/s10443-017-9623-7

39. Nayak, D., Bhatnagar, N., Mahajan, P.: Machining studies of UD-FRP composite part 2: finite element analysis. Mach. Sci. Technol. **9**(4), 503–528 (2005)

40. Turki, Y., Habak, M., Velasco, R., Aboura, Z., Khellil, K., Vantomme, P.: Experimental investigation of drilling damage and stitching effects on the mechanical behavior of carbon/epoxy composites. J. Mach. Tools. Manuf. **87**, 61–72 (2014)

41. Turki, Y., Habak, M., Velasco, R., Vantomme, P.: Highlighting cutting mechanisms encountered in carbon/epoxy composite drilling using orthogonal cutting. Int. J. Adv. Manuf. Technol. **92**(1–4), 685–697 (2017)
42. Su, Y., Jia, Z., Niu, B., Bi, G.: Size effect of depth of cut on chip formation mechanism in machining of CFRP. Compos. Struct. **164**, 316–327 (2017)
43. Li, H., Qin, X., He, G., Jin, Y., Sun, D., Price, M.: Investigation of chip formation and fracture toughness in orthogonal cutting of UD-CFRP. Int. J. Adv. Manuf. Technol. **82**(5–8), 1079–1088 (2016)